ZAMM · Z. Angew. Math. Mech. **90**, No. 5, 399 – 417 (2010) / **DOI** 10.1002/zamm.200900352

Generalization of one-dimensional material models for the finite element method

Michael Freund[1] **and Jörn Ihlemann**[2,*]

[1] German Institute of Rubber Technology, Eupener Str. 33, 30519 Hannover, Germany
[2] Chemnitz University of Technology, Mechanics of Solids, 09111 Chemnitz, Germany

Received 21 August 2009, revised 22 January 2010, accepted 12 February 2010
Published online 23 April 2010

Key words Constitutive modelling, representative directions, finite element implementation.

The concept of representative directions is intended to generalize one-dimensional material models for uniaxial tension to complete three-dimensional constitutive models for the finite element method. The concept is applicable to any model which is able to describe uniaxial loadings, even to those for inelastic material behavior without knowing the free energy. The typical characteristics of the respected material class are generalized in a remarkable similarity to the input model. The algorithm has already been implemented into the finite element systems ABAQUS and MSC.MARC considering several methods to increase the numerical efficiency. The implementation enables finite element simulations of inhomogeneous stress conditions within technical components, though the input model predicts uniaxial material behavior only.

1 Introduction

The simulation of technical components with regard to their mechanical behavior is basically achieved by means of the finite element method. Thus, for any particular material class a constitutive model is needed that is able to predict the complete correlation between the given state of strain and the corresponding state of stress while also considering the loading history in case of inelastic materials like elastomers. In general, this is equivalent to the input of six independent coefficients of the strain tensor to the user subroutine of the finite element program and the output of six stress values of the corresponding stress tensor.

The development of such a three-dimensional constitutive model might become a difficult task, but it often leads to an intermediate stage that at least enables the prediction of the material behavior for some specific loading processes such as uniaxial tension. Examples of those situations could be the extension of an elastic material model concerning inelastic effects or the translation of relations from physics to continuum mechanics (e.g. Heinrich et al. [7], Seelecke [17]). In such a situation it would be a great advantage to find a sufficient approximation of the prospective general behavior of a constitutive model by considering the uniaxial material behavior only. This is the idea of the so-called concept of representative directions which has primarily been developed for industrial applications.

The algorithm is based on the selection of evenly distributed directions in space which are used to identify the corresponding elongations due to an external deformation of the material point. The resulting uniaxial stress responses along those representative directions are given by the one-dimensional material model that is to be generalized. Then the next step is to postulate that the sum of stress powers of all uniaxial tension processes equals the stress power of the overall deformation process itself. This leads to a formula for calculating the unknown stress tensor which is to be interpreted as the response to the external deformation of the material point given by the corresponding strain tensor.

The typical material characteristics are generalized in a remarkable similarity to the input model, even though there remains a certain quantitative difference. As a consequence the parameter values of the generalized material model slightly differ from the parameters of the input model. But in fact this is not problematic since later on only the three-dimensional output model will be adapted to measurements for identifying the corresponding material parameters which are usually found in a comparable range.

From a mathematical point of view the concept of representative directions is quite similar to the micro-sphere model (Miehe et al. [13], but in fact the intention is somewhat different. Within the framework of the micro-sphere model the focus lies on the development of a micro-mechanical material model for a single polymer chain in a constrained environment

* Corresponding author E-mail: joern.ihlemann@mb.tu-chemnitz.de, Phone: +00 49 371 531 36946

by means of statistical physics. The transition to the mechanical behavior of the whole polymer network (micro-macro transition) is then achieved by averaging the energies of the single chains over different space orientations. This kind of homogenization technique was first introduced by Pawelski [15]. On the other hand the concept of representative directions is rather meant as a continuum mechanical generalization method without any reference to the physical structure of a polymer. The basic idea of this concept is the equivalence of stress power which leads to the average of vectorial force quantities instead of scalar energy quantities. Thus, the concept of representative directions is applicable to any inelastic material model without the need of knowing the free energy.

2 The concept of representative directions

2.1 Development of the constitutive model

During the loading process of a component there exists an individual state of deformation at each material point that is fully described by the deformation gradient $\underline{\underline{F}}$ (within the framework of idealization of continuum mechanics). This unsymmetric tensor maps a vector $\mathrm{d}\underline{\widetilde{r}}$ of infinitesimal length, which is tangent to any virtual line fixed to the material at the considered point, to a vector

$$\mathrm{d}\underline{r} = \underline{\underline{F}} \cdot \mathrm{d}\underline{\widetilde{r}} \tag{2.1}$$

co-deformed with the material. This relation can be used to determine the elongation

$$\lambda = \frac{|\mathrm{d}\underline{r}|}{|\mathrm{d}\underline{\widetilde{r}}|} = \sqrt{\frac{\mathrm{d}\underline{r} \cdot \mathrm{d}\underline{r}}{\mathrm{d}\underline{\widetilde{r}} \cdot \mathrm{d}\underline{\widetilde{r}}}} = \sqrt{\frac{\mathrm{d}\underline{\widetilde{r}} \cdot \underline{\underline{F}}^T \cdot \underline{\underline{F}} \cdot \mathrm{d}\underline{\widetilde{r}}}{\mathrm{d}\underline{\widetilde{r}} \cdot \mathrm{d}\underline{\widetilde{r}}}} = \sqrt{\frac{\mathrm{d}\underline{\widetilde{r}}}{\sqrt{\mathrm{d}\underline{\widetilde{r}} \cdot \mathrm{d}\underline{\widetilde{r}}}} \cdot \underline{\underline{F}}^T \cdot \underline{\underline{F}} \cdot \frac{\mathrm{d}\underline{\widetilde{r}}}{\sqrt{\mathrm{d}\underline{\widetilde{r}} \cdot \mathrm{d}\underline{\widetilde{r}}}}} \tag{2.2}$$

of such a material line along the direction of $\mathrm{d}\underline{\widetilde{r}}$ in the reference configuration. The expression $\underline{\underline{F}}^T \cdot \underline{\underline{F}}$ is equivalent to the symmetric Lagrangean right Cauchy-Green tensor $\underline{\underline{C}}$. Unlike the deformation gradient this tensor describes the pure state of strain of the material point. The last term also contains the unit vectors characterizing the direction of the elongated material lines in the undeformed configuration. To identify those individual directions the index α is used in the following way:

$$\overset{\alpha}{\underline{e}} = \frac{\mathrm{d}\underline{\widetilde{r}}}{\sqrt{\mathrm{d}\underline{\widetilde{r}} \cdot \mathrm{d}\underline{\widetilde{r}}}} \quad \Rightarrow \quad \overset{\alpha}{\lambda} = \lambda\left(\overset{\alpha}{\underline{e}}\right) = \sqrt{\overset{\alpha}{\underline{e}} \cdot \underline{\underline{C}} \cdot \overset{\alpha}{\underline{e}}} \quad . \tag{2.3}$$

Within a real material all those material lines are not purely elongated in their own direction but loaded in a more complex manner in so far as they interact with each other. Within the concept of representative directions these interactions are essentially simplified. However, they are not neglected at all because the elongations of the material lines are coupled by the given deformation of the material point. This is well illustrated in Eq. (2.3) where each elongation $\overset{\alpha}{\lambda}$ is calculated using the same strain tensor $\underline{\underline{C}}$ with its six independent coefficients. In other words it could be said, that with the given elongations of six material lines, the elongation of any other line is clearly determined.

The idea that each material line is assumed to react exclusively to the elongation calculated from the current state of deformation was first devised by Pawelski [15] and later on adopted by Lulei [12] and Miehe et al. [13]. All of them compute a contribution

$$\overset{\alpha}{f} = \overset{\alpha}{f}(\vartheta, \varphi) = \overset{\alpha}{f}\left(\overset{\alpha}{\lambda}(\vartheta, \varphi)\right) \quad \text{with} \quad \overset{\alpha}{\lambda}(\vartheta, \varphi) = \overset{\alpha}{\lambda}\left(\overset{\alpha}{\underline{e}}(\vartheta, \varphi)\right) \tag{2.4}$$

to the free energy for each material line, whereas this contribution only depends on the associated elongation and its history as a function of the spherical coordinates ϑ and φ. After that, the contributions of all directions in space are integrated to the total free energy f concerning the respective material point, whereas the differentiation of that energy with respect to the right Cauchy-Green tensor $\underline{\underline{C}}$ finally yields the demanded second Piola-Kirchhoff stress tensor $\underline{\underline{\widetilde{T}}}$:

$$f = \frac{1}{4\pi} \int_0^{2\pi} \int_0^{\pi} \overset{\alpha}{f} \sin\vartheta \, \mathrm{d}\vartheta \, \mathrm{d}\varphi \quad \Rightarrow \quad \underline{\underline{\widetilde{T}}} = 2 \, \frac{\partial f}{\partial \underline{\underline{C}}} \quad . \tag{2.5}$$

So far, the approach is useful for special material descriptions only because the stresses must be completely predictable by the free energy. This applies to ideal elasticity and some special types of inelastic material descriptions. However, this relation is not valid for all other material classes in general. The easiest example is a dashpot which in fact provides a

stress response but does not exhibit a free energy at all. But even more complex inelastic constitutive models like the MORPH model (Ihlemann [10]) are often based directly on stress relations without being derived from a corresponding energy. The concept of representative directions overcomes these restrictions by using vectorial force quantities instead of scalar energy quantities. For each individual direction $\overset{\alpha}{\underline{e}}$ the corresponding elongation $\overset{\alpha}{\lambda}$ is used to calculate a uniaxial first Piola-Kirchhoff stress response

$$\overset{\alpha}{T} = \overset{\alpha}{T}\left(\overset{\alpha}{\lambda}, \dot{\overset{\alpha}{\lambda}}, \ldots\right) \tag{2.6}$$

according to the one-dimensional material model that is intended to be generalized to a full three-dimensional constitutive model. For the further steps (see Eq. (2.9)) it is useful to switch to second Piola-Kirchhoff stresses

$$\overset{\alpha}{\widetilde{T}} = \frac{\overset{\alpha}{T}}{\overset{\alpha}{\lambda}} \quad . \tag{2.7}$$

The remaining task is to identify the unknown stress tensor $\underline{\underline{\widetilde{T}}}$ that corresponds to the current state of strain of the material point given by the right Cauchy-Green tensor $\underline{\underline{C}}$. For this purpose the definition of the stress power

$$\mathrm{d}P = \underline{\underline{\widetilde{T}}} \cdot\cdot\, \overset{\triangle}{\underline{\widetilde{\gamma}}}\, \mathrm{d}\widetilde{V} = \underline{\underline{T}} \cdot\cdot\, \overset{\triangle}{\underline{\underline{F}}}\, \mathrm{d}\widetilde{V} \quad \text{with} \quad \underline{\gamma} = \frac{1}{2}\left(\underline{\underline{C}} - \underline{\underline{I}}\right) \tag{2.8}$$

concerning an infinitesimal volume $\mathrm{d}\widetilde{V}$ of the material point in the reference configuration is used. The basic idea of the concept of representative directions is that the sum of stress powers of all uniaxial tension processes is set to be equal to the stress power of the deformation process concerning the whole material point:

$$\mathrm{d}P = \underline{\underline{\widetilde{T}}} \cdot\cdot\, \overset{\triangle}{\underline{\widetilde{\gamma}}}\, \mathrm{d}\widetilde{V} \overset{!}{=} \int_{\varphi}\int_{\vartheta} \overset{\alpha}{T}\, \dot{\overset{\alpha}{\lambda}}\, \mathrm{d}\overset{\alpha}{\widetilde{V}} = \int_{\varphi}\int_{\vartheta} \overset{\alpha}{\widetilde{T}}\, \overset{\alpha}{\lambda}\, \dot{\overset{\alpha}{\lambda}}\, \mathrm{d}\overset{\alpha}{\widetilde{V}} \tag{2.9}$$

$$\Rightarrow \underline{\underline{\widetilde{T}}} \cdot\cdot\, \overset{\triangle}{\underline{\widetilde{\gamma}}} = \int_{\varphi}\int_{\vartheta} \overset{\alpha}{\widetilde{T}}\, \overset{\alpha}{\lambda}\, \dot{\overset{\alpha}{\lambda}}\, \frac{\mathrm{d}\overset{\alpha}{\widetilde{V}}}{\mathrm{d}\widetilde{V}} \quad \text{with} \quad \frac{\mathrm{d}\overset{\alpha}{\widetilde{V}}}{\mathrm{d}\widetilde{V}} = \frac{\mathrm{d}\overset{\alpha}{\widetilde{A}}}{\mathrm{d}\widetilde{A}} = w\,\frac{\sin\vartheta\,\mathrm{d}\vartheta\,\mathrm{d}\varphi}{4\pi} \tag{2.10}$$

$$\Rightarrow \underline{\underline{\widetilde{T}}} \cdot\cdot\, \overset{\triangle}{\underline{\widetilde{\gamma}}} = \frac{w}{4\pi}\int_{0}^{2\pi}\int_{0}^{\pi} \overset{\alpha}{\widetilde{T}}\, \overset{\alpha}{\lambda}\, \dot{\overset{\alpha}{\lambda}}\, \sin\vartheta\,\mathrm{d}\vartheta\,\mathrm{d}\varphi \quad . \tag{2.11}$$

The expression $\mathrm{d}\overset{\alpha}{\widetilde{V}}/\mathrm{d}\widetilde{V}$ results from the idea that each material line with the direction $\overset{\alpha}{\underline{e}}$ has an associated volume $\mathrm{d}\overset{\alpha}{\widetilde{V}}$ as part of the volume $\mathrm{d}\widetilde{V}$ of the whole unit sphere so that the sphere is completely filled with these subvolumes. Finally, this proportion is additionally scaled with a constant faktor w that is equal for each direction in space. The free choice of this parameter enables the adaptation of the material tangent of the generalized constitutive model to the tangent of the one-dimensional input model concerning the reference configuration (see Eq. (2.39)). As a consequence the sum of all subvolumes is no longer equal to the volume of the unit sphere, but in fact this does not violate any physical laws. By means of Eqs. (2.3) and (2.8) the time derivative of the elongation

$$\dot{\overset{\alpha}{\lambda}} = \frac{1}{2\overset{\alpha}{\lambda}}\, \overset{\alpha}{\underline{e}} \cdot \overset{\triangle}{\underline{\underline{C}}} \cdot \overset{\alpha}{\underline{e}} = \frac{1}{\overset{\alpha}{\lambda}}\, \overset{\alpha}{\underline{e}} \circ \overset{\alpha}{\underline{e}} \cdot\cdot\, \frac{1}{2}\overset{\triangle}{\underline{\underline{C}}} = \frac{1}{\overset{\alpha}{\lambda}}\, \overset{\alpha}{\underline{e}} \circ \overset{\alpha}{\underline{e}} \cdot\cdot\, \overset{\triangle}{\underline{\gamma}} \tag{2.12}$$

can be specified. Inserting this expression into Eq. (2.11) finally leads to a definition for the demanded second Piola-Kirchhoff stress tensor $\underline{\underline{\widetilde{T}}}$ that is to be interpreted as the response to the state of strain within the material point given by the right Cauchy-Green tensor $\underline{\underline{C}}$:

$$\underline{\underline{\widetilde{T}}} \cdot\cdot\, \overset{\triangle}{\underline{\widetilde{\gamma}}} = \frac{w}{4\pi}\int_{0}^{2\pi}\int_{0}^{\pi} \overset{\alpha}{\widetilde{T}}\, \overset{\alpha}{\underline{e}} \circ \overset{\alpha}{\underline{e}}\, \sin\vartheta\,\mathrm{d}\vartheta\,\mathrm{d}\varphi \cdot\cdot\, \overset{\triangle}{\underline{\gamma}} \quad \Rightarrow \quad \underline{\underline{\widetilde{T}}} = \frac{w}{4\pi}\int_{0}^{2\pi}\int_{0}^{\pi} \overset{\alpha}{\widetilde{T}}\, \overset{\alpha}{\underline{e}} \circ \overset{\alpha}{\underline{e}}\, \sin\vartheta\,\mathrm{d}\vartheta\,\mathrm{d}\varphi \quad . \tag{2.13}$$

Obviously the term $\overset{\alpha}{\widetilde{T}}\, \overset{\alpha}{\underline{e}} \circ \overset{\alpha}{\underline{e}}$ represents a complete stress tensor of the virtual uniaxial tension process along the individual direction $\overset{\alpha}{\underline{e}}$, whereas the averaging of all these tensors generates a complete three-dimensional constitutive model for

the given one-dimensional material behavior. Apart from one special case (see Eq. (3.1)) the integral over continuously distributed directions in space cannot be solved analytically, so that a numerical integration has to be done instead. For this purpose the integrand $\overset{\alpha}{\widetilde{T}}\,\underline{\overset{\alpha}{e}}\circ\underline{\overset{\alpha}{e}}$ is scaled with appropriate weighting factors $\overset{\alpha}{w}$ according to Eq. (2.10) and summed up over a discrete number of representative directions as an extract of the infinite number of continuously distributed directions in space:

$$\underline{\underline{\widetilde{T}}} = \sum_{\alpha=1}^{n} \overset{\alpha}{w}\,\overset{\alpha}{\widetilde{T}}\,\underline{\overset{\alpha}{e}}\circ\underline{\overset{\alpha}{e}} \quad \text{with} \quad \overset{\alpha}{w} = w\,\frac{\Delta\overset{\alpha}{\widetilde{V}}}{\widetilde{V}_{\text{Sphere}}} = w\,\frac{\Delta\overset{\alpha}{\widetilde{A}}}{\widetilde{A}_{\text{Sphere}}} \quad . \tag{2.14}$$

Finally, the conversion of the dyads $\underline{\overset{\alpha}{e}}\circ\underline{\overset{\alpha}{e}}$ into a cartesian coordinate system allows the calculation of the coefficients

$$\widetilde{T}_{ab} = \underline{e}_a\cdot\underline{\underline{\widetilde{T}}}\cdot\underline{e}_b = \sum_{\alpha=1}^{n}\overset{\alpha}{w}\,\overset{\alpha}{\widetilde{T}}\left(\underline{e}_a\cdot\underline{\overset{\alpha}{e}}\right)\left(\underline{\overset{\alpha}{e}}\cdot\underline{e}_b\right) = \sum_{\alpha=1}^{n}\overset{\alpha}{w}\,\overset{\alpha}{\widetilde{T}}\,\overset{\alpha}{e}_a\,\overset{\alpha}{e}_b \quad . \tag{2.15}$$

2.2 Linearization

In this section the tensorial material model of Eq. (2.13) is about to be verified concerning some aspects of plausibility. For this purpose it will be checked whether the linearization of this three-dimensional stress-strain behavior corresponds with Hooke's law considering the typical characteristics of its material parameters. The first step of linearizing the constitutive model is to derive the material tangent

$$\underline{\underline{\underline{\underline{K}}}} = \frac{\partial\underline{\underline{\widetilde{T}}}}{\partial\underline{\underline{\gamma}}} = \frac{w}{4\pi}\int_0^{2\pi}\int_0^{\pi}\underline{\overset{\alpha}{e}}\circ\underline{\overset{\alpha}{e}}\circ\frac{\partial\overset{\alpha}{\widetilde{T}}}{\partial\underline{\underline{\gamma}}}\,\sin\vartheta\,\mathrm{d}\vartheta\,\mathrm{d}\varphi = \frac{w}{4\pi}\int_0^{2\pi}\int_0^{\pi}\underline{\overset{\alpha}{e}}\circ\underline{\overset{\alpha}{e}}\circ\frac{\partial\overset{\alpha}{\widetilde{T}}}{\partial\overset{\alpha}{\lambda}}\frac{\partial\overset{\alpha}{\lambda}}{\partial\underline{\underline{\gamma}}}\,\sin\vartheta\,\mathrm{d}\vartheta\,\mathrm{d}\varphi \tag{2.16}$$

as a tensor of fourth order. In this context the one-dimensional input model is assumed to be fully elastic, so that the uniaxial stresses $\overset{\alpha}{\widetilde{T}}$ exclusively depend on the elongations $\overset{\alpha}{\lambda}$. For the further steps the elongation $\overset{\alpha}{\lambda}$ is replaced by the expression in Eq. (2.3), whereas the right Cauchy-Green tensor $\underline{\underline{C}}$ is associated with the Green-Lagrange strain tensor $\underline{\underline{\gamma}}$ according to Eq. (2.8):

$$\begin{aligned}
\underline{\underline{\underline{\underline{K}}}} &= \frac{w}{4\pi}\int_0^{2\pi}\int_0^{\pi}\underline{\overset{\alpha}{e}}\circ\underline{\overset{\alpha}{e}}\circ\frac{\partial\overset{\alpha}{\widetilde{T}}}{\partial\overset{\alpha}{\lambda}}\frac{\partial\left(\sqrt{\underline{\overset{\alpha}{e}}\cdot\underline{\underline{C}}\cdot\underline{\overset{\alpha}{e}}}\right)}{\partial\underline{\underline{\gamma}}}\,\sin\vartheta\,\mathrm{d}\vartheta\,\mathrm{d}\varphi \\
&= \frac{w}{4\pi}\int_0^{2\pi}\int_0^{\pi}\underline{\overset{\alpha}{e}}\circ\underline{\overset{\alpha}{e}}\circ\frac{\partial\overset{\alpha}{\widetilde{T}}}{\partial\overset{\alpha}{\lambda}}\frac{1}{2\overset{\alpha}{\lambda}}\frac{\partial\left(\underline{\overset{\alpha}{e}}\cdot\underline{\underline{C}}\cdot\underline{\overset{\alpha}{e}}\right)}{\partial\underline{\underline{\gamma}}}\,\sin\vartheta\,\mathrm{d}\vartheta\,\mathrm{d}\varphi \\
&= \frac{w}{4\pi}\int_0^{2\pi}\int_0^{\pi}\underline{\overset{\alpha}{e}}\circ\underline{\overset{\alpha}{e}}\circ\frac{\partial\overset{\alpha}{\widetilde{T}}}{\partial\overset{\alpha}{\lambda}}\frac{1}{\overset{\alpha}{\lambda}}\frac{\partial\left(\underline{\overset{\alpha}{e}}\cdot\underline{\underline{\gamma}}\cdot\underline{\overset{\alpha}{e}}\right)}{\partial\underline{\underline{\gamma}}}\,\sin\vartheta\,\mathrm{d}\vartheta\,\mathrm{d}\varphi \\
&= \frac{w}{4\pi}\int_0^{2\pi}\int_0^{\pi}\underline{\overset{\alpha}{e}}\circ\underline{\overset{\alpha}{e}}\circ\frac{\partial\overset{\alpha}{\widetilde{T}}}{\partial\overset{\alpha}{\lambda}}\frac{1}{\overset{\alpha}{\lambda}}\frac{\partial\left(\underline{\overset{\alpha}{e}}\circ\underline{\overset{\alpha}{e}}\cdot\cdot\,\underline{\underline{\gamma}}\right)}{\partial\underline{\underline{\gamma}}}\,\sin\vartheta\,\mathrm{d}\vartheta\,\mathrm{d}\varphi \quad .
\end{aligned} \tag{2.17}$$

The derivative of $\left(\underline{\overset{\alpha}{e}}\circ\underline{\overset{\alpha}{e}}\cdot\cdot\,\underline{\underline{\gamma}}\right)$ results as follows (e.g. Holzapfel [9], Ihlemann [11])):

$$\frac{\partial\left(\underline{\overset{\alpha}{e}}\circ\underline{\overset{\alpha}{e}}\cdot\cdot\,\underline{\underline{\gamma}}\right)}{\partial\underline{\underline{\gamma}}} = \underline{\overset{\alpha}{e}}\circ\underline{\overset{\alpha}{e}}\cdot\cdot\frac{\partial\underline{\underline{\gamma}}}{\partial\underline{\underline{\gamma}}} = \underline{\overset{\alpha}{e}}\circ\underline{\overset{\alpha}{e}}\cdot\cdot\,\frac{1}{2}\left(\underline{e}_a\circ\underline{e}_b\circ\underline{e}_a\circ\underline{e}_b + \underline{e}_a\circ\underline{e}_b\circ\underline{e}_b\circ\underline{e}_a\right) = \underline{\overset{\alpha}{e}}\circ\underline{\overset{\alpha}{e}} \quad . \tag{2.18}$$

Inserting this expression into Eq. (2.17) leads to the final tensorial formulation for the material tangent

$$\underline{\underline{\underline{\underline{K}}}} = \frac{w}{4\pi}\int_0^{2\pi}\int_0^{\pi}\frac{\partial\overset{\alpha}{\widetilde{T}}}{\partial\overset{\alpha}{\lambda}}\frac{1}{\overset{\alpha}{\lambda}}\,\underline{\overset{\alpha}{e}}\circ\underline{\overset{\alpha}{e}}\circ\underline{\overset{\alpha}{e}}\circ\underline{\overset{\alpha}{e}}\,\sin\vartheta\,\mathrm{d}\vartheta\,\mathrm{d}\varphi \quad . \tag{2.19}$$

By using the basis vectors $\underline{e}_a$ of a cartesian coordinate system the coefficients of the material tangent

$$\begin{aligned} K_{abcd} &= \underline{e}_b \circ \underline{e}_a \cdot\cdot \underline{\underline{\underline{K}}} \cdot\cdot \underline{e}_d \circ \underline{e}_c \\ &= \frac{w}{4\pi} \int_0^{2\pi} \int_0^{\pi} \frac{\partial \overset{\alpha}{\widetilde{T}}}{\partial \overset{\alpha}{\lambda}} \frac{1}{\overset{\alpha}{\lambda}} \left(\underline{e}_a \cdot \overset{\alpha}{\underline{e}}\right) \left(\underline{e}_b \cdot \overset{\alpha}{\underline{e}}\right) \left(\underline{e}_c \cdot \overset{\alpha}{\underline{e}}\right) \left(\underline{e}_d \cdot \overset{\alpha}{\underline{e}}\right) \sin\vartheta \, \mathrm{d}\vartheta \, \mathrm{d}\varphi \\ &= \frac{w}{4\pi} \int_0^{2\pi} \int_0^{\pi} \frac{\partial \overset{\alpha}{\widetilde{T}}}{\partial \overset{\alpha}{\lambda}} \frac{1}{\overset{\alpha}{\lambda}} \overset{\alpha}{e}_a \overset{\alpha}{e}_b \overset{\alpha}{e}_c \overset{\alpha}{e}_d \sin\vartheta \, \mathrm{d}\vartheta \, \mathrm{d}\varphi \end{aligned} \tag{2.20}$$

can be determined (see Eq. (2.15)). As an example a linear relation between the uniaxial stresses $\overset{\alpha}{T}$ and the corresponding elongations $\overset{\alpha}{\lambda}$, which can also be interpreted as the one-dimensional formulation of Hooke's law, will be used in the following:

$$\overset{\alpha}{T} = c \left(\overset{\alpha}{\lambda} - 1\right) \quad \Rightarrow \quad \overset{\alpha}{\widetilde{T}} = c \left(1 - \frac{1}{\overset{\alpha}{\lambda}}\right) \quad \Rightarrow \quad \frac{\partial \overset{\alpha}{\widetilde{T}}}{\partial \overset{\alpha}{\lambda}} = \frac{c}{\overset{\alpha}{\lambda^2}} \quad . \tag{2.21}$$

Thus, the coefficients for this one-dimensional material behavior are given by

$$K_{abcd} = \frac{cw}{4\pi} \int_0^{2\pi} \int_0^{\pi} \frac{1}{\overset{\alpha}{\lambda^3}} \overset{\alpha}{e}_a \overset{\alpha}{e}_b \overset{\alpha}{e}_c \overset{\alpha}{e}_d \sin\vartheta \, \mathrm{d}\vartheta \, \mathrm{d}\varphi \quad . \tag{2.22}$$

The material tangent referring to the reference configuration can be derived by using the identity tensor $\underline{\underline{I}}$ as the current state of strain (see Eq. (2.3)):

$$\underline{\underline{\underline{\widetilde{K}}}} = \underline{\underline{\underline{K}}} \left(\underline{\underline{C}} = \underline{\underline{I}}\right) \quad \Rightarrow \quad \widetilde{K}_{abcd} = \frac{cw}{4\pi} \int_0^{2\pi} \int_0^{\pi} \overset{\alpha}{e}_a \overset{\alpha}{e}_b \overset{\alpha}{e}_c \overset{\alpha}{e}_d \sin\vartheta \, \mathrm{d}\vartheta \, \mathrm{d}\varphi \quad . \tag{2.23}$$

Considering the dependence of the coefficients $\overset{\alpha}{e}_a$ on the spherical coordinates ϑ and φ the solution of the double integral yields the following linearized constitutive model as the generalization of the one-dimensional stress-strain relation of Eq. (2.21):

$$\underline{\underline{\widetilde{T}}} = \underline{\underline{\underline{\widetilde{K}}}} \cdot\cdot \underline{\underline{\gamma}} \quad \Rightarrow \quad \begin{bmatrix} \widetilde{T}_{xx} \\ \widetilde{T}_{yy} \\ \widetilde{T}_{zz} \\ \sqrt{2}\widetilde{T}_{xy} \\ \sqrt{2}\widetilde{T}_{yz} \\ \sqrt{2}\widetilde{T}_{xz} \end{bmatrix} = \frac{c\,w}{15} \begin{bmatrix} 3 & 1 & 1 & 0 & 0 & 0 \\ 1 & 3 & 1 & 0 & 0 & 0 \\ 1 & 1 & 3 & 0 & 0 & 0 \\ 0 & 0 & 0 & 2 & 0 & 0 \\ 0 & 0 & 0 & 0 & 2 & 0 \\ 0 & 0 & 0 & 0 & 0 & 2 \end{bmatrix} \cdot \begin{bmatrix} \gamma_{xx} \\ \gamma_{yy} \\ \gamma_{zz} \\ \sqrt{2}\,\gamma_{xy} \\ \sqrt{2}\,\gamma_{yz} \\ \sqrt{2}\,\gamma_{xz} \end{bmatrix} \quad . \tag{2.24}$$

Because of their symmetry the stress tensor and the strain tensor can be reduced to six independent coefficients, so that the material tangent is fully described by 21 independent stiffness values. According to Hooke's law the shear modulus G is determined by the correlation between the shear strain ε_{xy} and the associated stress response σ_{xy}. In case of infinitesimal deformations concerning the reference configuration the Cauchy stresses σ and the linearized strains ε coincide with the Lagrangean quantities $\widetilde{T}$ and γ, so that

$$\widetilde{T}_{xy} = 2\,G\,\gamma_{xy} \quad \text{and} \quad G = \frac{c\,w}{15} \quad . \tag{2.25}$$

The bulk modulus can be derived from the hydrostatic pressure

$$p = -\frac{1}{3} \operatorname{tr}\left(\underline{\underline{\widetilde{T}}}\right) = -\frac{1}{3}\left(\widetilde{T}_{xx} + \widetilde{T}_{yy} + \widetilde{T}_{zz}\right) = -\frac{cw}{9}\left(\gamma_{xx} + \gamma_{yy} + \gamma_{zz}\right) \quad , \tag{2.26}$$

whereas the trace of the stress tensor can be replaced by the coefficients of the strain tensor considering Eq. (2.24). The sum of the strain coefficients is equivalent to the linearized volume strain which relates to the hydrostatic pressure p according to the bulk modulus K:

$$p = -K\,\frac{\Delta V}{\widetilde{V}} \quad \Rightarrow \quad K = \frac{c\,w}{9} \quad . \tag{2.27}$$

The calculation of the remaining elasticity constants can be accomplished by converting Eq. (2.24) to the coefficients

$$\begin{bmatrix} \gamma_{xx} \\ \gamma_{yy} \\ \gamma_{zz} \\ \sqrt{2}\,\gamma_{xy} \\ \sqrt{2}\,\gamma_{yz} \\ \sqrt{2}\,\gamma_{xz} \end{bmatrix} = \frac{15}{c\,w} \begin{bmatrix} 2/5 & -1/10 & -1/10 & 0 & 0 & 0 \\ -1/10 & 2/5 & -1/10 & 0 & 0 & 0 \\ -1/10 & -1/10 & 2/5 & 0 & 0 & 0 \\ 0 & 0 & 0 & 1/2 & 0 & 0 \\ 0 & 0 & 0 & 0 & 1/2 & 0 \\ 0 & 0 & 0 & 0 & 0 & 1/2 \end{bmatrix} \cdot \begin{bmatrix} \widetilde{T}_{xx} \\ \widetilde{T}_{yy} \\ \widetilde{T}_{zz} \\ \sqrt{2}\,\widetilde{T}_{xy} \\ \sqrt{2}\,\widetilde{T}_{yz} \\ \sqrt{2}\,\widetilde{T}_{xz} \end{bmatrix} \tag{2.28}$$

of the Green-Lagrange strain tensor $\underline{\underline{\gamma}}$. The consideration of the boundary conditions for uniaxial tension ($\widetilde{T}_{yy} = \widetilde{T}_{zz} = 0$) allows the specification of the elastic modulus:

$$\gamma_{xx} = \frac{\widetilde{T}_{xx}}{E} \quad \Rightarrow \quad E = \frac{c\,w}{6} \quad . \tag{2.29}$$

Finally, the Poisson's ratio ν is determined by the following equation according to Hooke's law:

$$\gamma_{xx} = \frac{1}{E}\left[\widetilde{T}_{xx} - \nu\left(\widetilde{T}_{yy} + \widetilde{T}_{zz}\right)\right] \quad \Rightarrow \quad \nu = \frac{1}{4} \quad . \tag{2.30}$$

This result shows a significant difference compared to the original Hooke's law where the Poisson's ratio is an arbitrary material parameter. Obviously the concept of representative directions produces a constant value for the parameter ν which does not depend on the uniaxial input model, so that the generalized constitutive model is always characterized by a compressible material behavior. This results from the fact that the reaction due to lateral contraction cannot be identified from the one-dimensional stress-strain relation. Nevertheless the typical correlations between the elastic constants of Hooke's law are also valid for the linearized constitutive model resulting from the concept of representative directions:

$$G = \frac{E}{2\,(1+\nu)} \quad , \quad K = \frac{E}{3\,(1-2\nu)} \quad \Rightarrow \quad E = \frac{9KG}{G+3K} \quad . \tag{2.31}$$

2.3 Adaptation to quasi incompressible materials

The constant Poisson's ratio of $\nu = 1/4$ of the linearized constitutive model means a serious restriction with respect to the application of the concept because the resulting material behavior concerning hydrostatic loads cannot be adjusted to the particular material class that is represented by the one-dimensional input model. As a consequence the concept is not yet applicable to almost incompressible materials like elastomers. To overcome this restriction the algorithm has to be extended in such a way that the concept itself is limited to pure isochoric deformations while the stress response concerning volume strains is to be modeled separately. Thus, the first step is to calculate the elongations

$$\overset{G}{\underset{\alpha}{\lambda}} = \sqrt{\underline{\underline{e}}^{\alpha} \cdot \overset{G}{\underline{\underline{C}}} \cdot \underline{\underline{e}}^{\alpha}} \tag{2.32}$$

merely with the isochoric right Cauchy-Green tensor $\overset{G}{\underline{\underline{C}}}$ (with $\overset{G}{\underline{\underline{C}}} = J_3^{-\frac{2}{3}}\,\underline{\underline{C}}$ and $J_3 = \det \underline{\underline{F}}$) which leads to a modified second Piola-Kirchhoff stress tensor

$$\widetilde{\underline{\underline{T}}}^{*} = \frac{w}{4\pi} \int_0^{2\pi} \int_0^{\pi} \overset{\alpha}{\widetilde{T}}\left(\overset{G}{\underset{\alpha}{\lambda}}\right) \underline{\underline{e}}^{\alpha} \circ \underline{\underline{e}}^{\alpha} \sin\vartheta \,\mathrm{d}\vartheta \,\mathrm{d}\varphi \quad . \tag{2.33}$$

This tensor, which still describes a compressible material behavior, does not correspond with the isochoric stress tensor $\overset{G}{\underline{\underline{T}}}$ because it still includes concealed hydrostatic Cauchy stresses as a result of the associated isochoric strain condition. Instead, according to Ihlemann [10] the isochoric stresses are given by

$$\overset{G}{\underline{\underline{T}}} = \left(\widetilde{\underline{\underline{T}}}^{*} \cdot \overset{G}{\underline{\underline{C}}}\right)' \cdot \overset{G}{\underline{\underline{C}}}^{-1} \quad . \tag{2.34}$$

On the other hand the volumetric stress tensor

$$\overset{V}{\underline{\underline{\widetilde{T}}}} = -J_3\, p\, \overset{V}{\underline{\underline{C}}}^{-1} \quad \text{with} \quad \overset{V}{\underline{\underline{C}}} = J_3^{\frac{2}{3}}\, \underline{\underline{I}} \tag{2.35}$$

depends on the hydrostatic pressure p as a function of the bulk modulus K and the volume ratio J_3. In those cases, where the resistance against volume changes is much higher than the resistance against isochoric strains, a linear function

$$p = -K\,(J_3 - 1) \tag{2.36}$$

for the hydrostatic pressure can be used. In contrast to the Eulerian Cauchy stress tensor $\underline{\underline{\sigma}}$ the Lagrangean second Piola-Kirchhoff stress tensor $\underline{\underline{\widetilde{T}}}$ itself is not additively composed of an isochoric and volumetric part but the product

$$\underline{\underline{\widetilde{T}}} \cdot \underline{\underline{C}} = \overset{G}{\underline{\underline{\widetilde{T}}}} \cdot \overset{G}{\underline{\underline{C}}} + \overset{V}{\underline{\underline{\widetilde{T}}}} \cdot \overset{V}{\underline{\underline{C}}} \quad . \tag{2.37}$$

This leads to the final stress tensor

$$\underline{\underline{\widetilde{T}}} = \left(\underline{\underline{\widetilde{T}}}^{*} \cdot \overset{G}{\underline{\underline{C}}}\right)' \cdot \underline{\underline{C}}^{-1} - p\, J_3\, \underline{\underline{C}}^{-1} \tag{2.38}$$

of the extended constitutive model whose compressibility can be freely adjusted with the bulk modulus K as an additional arbitrary material parameter. The intermediate stress tensor $\underline{\underline{\widetilde{T}}}^{*}$ still includes the free parameter w as a part of the weighting factors $\overset{\alpha}{w}$ (see Eq. (2.14)). Thus, the next step is to determine this quantity in such a manner that the elastic modulus of the final constitutive model coincides with the material tangent of the one-dimensional input model concerning the undeformed configuration. The linearization of the extended constitutive model according to Eq. (2.38) yields the same shear modulus as already depicted in Eq. (2.25), so that in combination with Eq. (2.31) the free parameter w can be specified:

$$E \overset{!}{=} c \quad \Rightarrow \quad w = 15\,\frac{G}{E} = 15\,\frac{G\,(G+3K)}{9KG} \quad \Rightarrow \quad w = 5\left(1 + \frac{G}{3K}\right) \quad . \tag{2.39}$$

In this example the stiffness c refers to the linear stress-strain relation of Eq. (2.21), but this quantity can be replaced by the material tangent K_0 of any other input model as well, so that the formula is valid for any given one-dimensional material behavior. Thus, in case of almost incompressible material behavior ($K \gg G$) the parameter w is approximately 5.

3 Applications

The capability of the described algorithm can be tested by using already known three-dimensional constitutive models whose reduced material description for uniaxial tension serves as the one-dimensional input model for the concept of representative directions. As a result the concept produces a new constitutive model which is to be compared with the original tensorial model. In order to get an accurate numerical solution for the approximation of the integral over continuously distributed directions in space (see Eq. (2.13)) the generation of a large number of representative directions is required. For this purpose the unit sphere is to divide into longitudes and latitudes, whereas the unit vectors $\overset{\alpha}{\underline{e}}$ as representative directions point to the centers of the resulting subareas (used as weighting factors). In this context it is to be mentioned that this irregular distribution in combination with a large number of directions is only used for testing the concept where the computing time is less important. Of course the application of the concept concerning the finite element method requires a more efficient distribution of representative directions since the number of directions is to be reduced as much as possible (see Sect. 4.1).

3.1 Elastic material models

The first example for the uniaxial material model is a linear relation between the second Piola-Kirchhoff stresses $\overset{\alpha}{\widetilde{T}}$ and the Green-Lagrange strains $\overset{\alpha}{\gamma}$ as a reduction of the associated three-dimensional Hooke's law according to the Lagrangean formulation:

$$\underline{\underline{\widetilde{T}}} = \underline{\underline{\underline{\underline{K}}}} \cdot\cdot\, \underline{\underline{\gamma}} \quad \Rightarrow \quad \overset{\alpha}{\widetilde{T}} = c\,\overset{\alpha}{\gamma} \quad . \tag{3.1}$$

As far as known, this is the only case where the integral of Eq. (2.13) can be solved analytically and the given material behavior is completely reproduced by the concept of representative directions. Thus, the generalized material model coincides with the tensorial equivalent of the one-dimensional input model for a chosen Poisson's ratio of $\nu = 1/4$. Of course

this does only relate to the original concept by calculating the stress tensor $\underline{\underline{\widetilde{T}}}$ with the complete strain tensor $\underline{\underline{C}}$, whereas the extended concept with the separate calculation of the stress response due to hydrostatic loads (see Eq. (2.38)) leads to a modified material behavior. Concerning these two versions of the algorithm Fig. 3.1 illustrates the stress-strain curve (left) as well as the characteristic of the volume ratio J_3 (right) for a simulated uniaxial tension test.

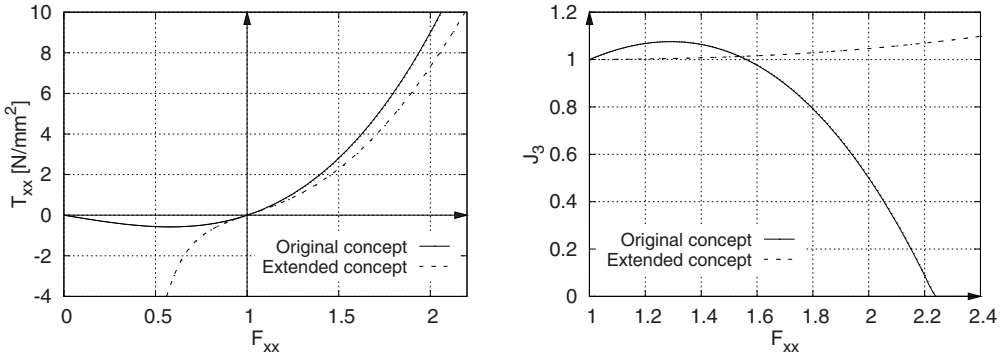

Fig. 3.1 Simulation of a uniaxial tension test with a linear Lagrangean stress-strain relation in representative directions using the original and the extended version of the algorithm.

Obviously the original Hooke's law is not suitable for large deformations because of the decreasing stress values for high compression on the one hand and the decreasing volume for even low tension on the other hand. In contrast to this the extended algorithm leads to a physically reasonable material behavior with respect to the characteristic of the stress response as well as the volume ratio. In this case the bulk modulus was chosen much higher than the shear modulus, so that the change of the volume is comparatively small. As a consequence of using the extended concept the resulting material behavior concerning tension differs quantitatively from the original material model but nevertheless the nonlinear characteristic has been completely retained during the process of generalization. These first results show that the concept of representative directions should be preferably applied to those kind of material models which already describe a reasonable material behavior on their own. Thus, the further examples will discuss material models especially used for elastomers for which the concept has originally been developed. For this purpose the incompressible Neo-Hooke model as the simplest hyperelastic material model is applied to the concept:

$$\underline{\underline{\widetilde{T}}} = 2\,C_{10}\left(\underline{\underline{I}} - \frac{1}{3}\,\mathrm{tr}\left(\underline{\underline{C}}\right)\underline{\underline{C}}^{-1}\right) - p\,\underline{\underline{C}}^{-1} \quad \Rightarrow \quad \overset{\alpha}{\widetilde{T}} = 2\,C_{10}\left(1 - \frac{1}{\overset{\alpha}{\lambda}{}^3}\right) \quad . \tag{3.2}$$

For the use within representative directions the one-dimensional material description of Neo-Hooke is derived from the associated tensorial formulation in case of ideal incompressibility, so that the material behavior concerning hydrostatic loads is to be adjusted exclusively by the bulk modulus of the generalized model. Fig. 3.2 shows the stress-strain curves for a simulated uniaxial tension test and a simple shear test using the original Neo-Hooke constitutive model and the generalized material model resulting from the concept of representative directions, whereas the material parameter C_{10} is chosen equally for both models.

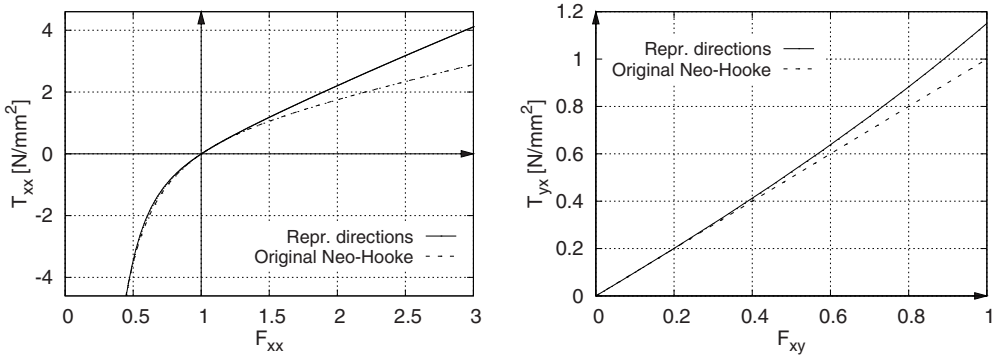

Fig. 3.2 Simulation of a uniaxial tension test and a simple shear test using the original Neo-Hooke constitutive model and the uniaxial Neo-Hooke model in representative directions.

Because of the simplified interactions between the representative directions the use of a constitutive model within that concept is just an approximation of the material behavior predicted by the original constitutive model itself, so that a quantitative agreement between both models is not to be expected at all. However, the qualitative material behavior has been transfered in a remarkable similarity which is much more important with respect to the application of the concept. In fact, the comparison between these two constitutive models only makes sense for testing the concept, but concerning a real application of the algorithm only the generalized material model will be adapted to measurements for identifying the material parameters. Thus, a certain quantitative difference compared to the input model is not crucial as long as the optimized material parameters are found in a physically reasonable range.

So far these first examples illustrate the effect of the described algorithm in case of ideal elasticity only. In this context the method used by Pawelski [15], which could be interpreted as a special case of the concept of representative directions, exactly produces the same material behavior. Thus, elastic material models only serve for testing the new algorithm, whereas its great advantage does not become obvious until using material models with distinctive inelastic characteristics.

3.2 Inelastic material models

A well suitable material model for testing the algorithm concerning inelastic characteristics is the so-called MORPH constitutive model (**MO**del of **R**ubber **PH**enomenology) which has originally been developed by Ihlemann [10] to describe the mechanical behavior of elastomers used in air springs. By identifying only eight material parameters this model is able to consider most of the quasi-static effects of rubber-like materials like hysteresis, Mullins effect, remaining strains, and nonlinearity due to large deformations. Concerning the Lagrangean formulation the total stress tensor of the MORPH model is composed of the following stress contributions:

$$\underline{\underline{\widetilde{T}}} = 2\,\alpha\,\underline{\underline{\overset{G}{C}}}' \cdot \underline{\underline{C}}^{-1} + \left(\underline{\underline{\widetilde{T}}}^{A} \cdot \underline{\underline{C}}\right)' \cdot \underline{\underline{C}}^{-1} - p\,J_3\,\underline{\underline{C}}^{-1} \quad . \tag{3.3}$$

The first part depends on the variable α (see Eq. (3.9)) which is a function of some of the eight material parameters p_i and

$$C_T^H = \max\left[\overset{G}{C}_T(\tau)\ ;\ 0 \le \tau \le t\right] \tag{3.4}$$

as the maximum value

$$\overset{G}{C}_T = \max\left[|\overset{G}{C}_I - \overset{G}{C}_J|\ ;\ I,J = 1,2,3\right] \tag{3.5}$$

of the Tresca invariant of the isochoric right Cauchy-Green-Tensor $\underline{\underline{\overset{G}{C}}}$ occurred during the whole loading history as a measure of the stress softening (Mullins Effect). As a consequence this part of the stress tensor describes an elastic material behavior once the maximum deformation has been reached. The second part of the total stresses is defined by a differential equation

$$\underline{\underline{\overset{\triangle}{\widetilde{T}}}}^{A} = \beta\,\overset{G}{L}_T\left(\underline{\underline{\widetilde{T}}}^{L} - \underline{\underline{\widetilde{T}}}^{A}\right) + \frac{1}{3}\left(\underline{\underline{\widetilde{T}}}^{A} \cdot\cdot\, \underline{\underline{C}}\right)\underline{\underline{\overset{\triangle}{C}}}^{-1} - \frac{1}{3}\left(\underline{\underline{C}}^{-1} \cdot\cdot\, \underline{\underline{\overset{\triangle}{C}}}\right)\underline{\underline{\widetilde{T}}}^{A} \tag{3.6}$$

for the additional stresses $\underline{\underline{\widetilde{T}}}^{A}$. The calculation of the limiting stresses

$$\underline{\underline{\widetilde{T}}}^{L} = \left(\gamma \exp\left(\left(p_7\,\frac{\underline{\underline{\overset{G}{L}}}}{\overset{G}{L}_T}\,\frac{\overset{G}{C}_T}{C_T^H}\right)\right) + p_8\,\frac{\underline{\underline{\overset{G}{L}}}}{\overset{G}{L}_T}\right) \cdot \underline{\underline{C}}^{-1} \tag{3.7}$$

requires the solution of an exponential function of the tensor

$$\underline{\underline{\overset{G}{L}}} = \frac{1}{2}\left(\underline{\underline{C}}^{-1} \cdot \underline{\underline{\overset{\triangle}{C}}} + \underline{\underline{\overset{\triangle}{C}}} \cdot \underline{\underline{C}}^{-1}\right)' \cdot \underline{\underline{\overset{G}{C}}} \tag{3.8}$$

which can be interpreted as the Lagrangean equivalent to the Zaremba-Jaumann time derivative of the isochoric left Cauchy-Green tensor $\underline{\underline{\overset{G}{b}}}$. Finally, the variables α, β, and γ are given by the following correlations:

$$\left.\begin{aligned} \alpha &= p_1 + p_2\,f\left(p_3\,C_T^H\right) \\ \beta &= p_4\,f\left(p_3\,C_T^H\right) \\ \gamma &= p_5\,C_T^H\left(1 - f\left(C_T^H/p_6\right)\right) \end{aligned}\right\} \quad \text{with} \quad f(x) = \frac{1}{\sqrt{1+x^2}} \quad . \tag{3.9}$$

To identify the eight material parameters the MORPH constitutive model has been simultaneously adapted to a uniaxial tension and a simple shear measurement of a carbon black filled chloroprene rubber while considering the stationary loading cycles only. Fig. 3.3 shows the simulation of these two loading processes based on a common set of optimized material parameters as well as the corresponding measurements (Ihlemann [10]).

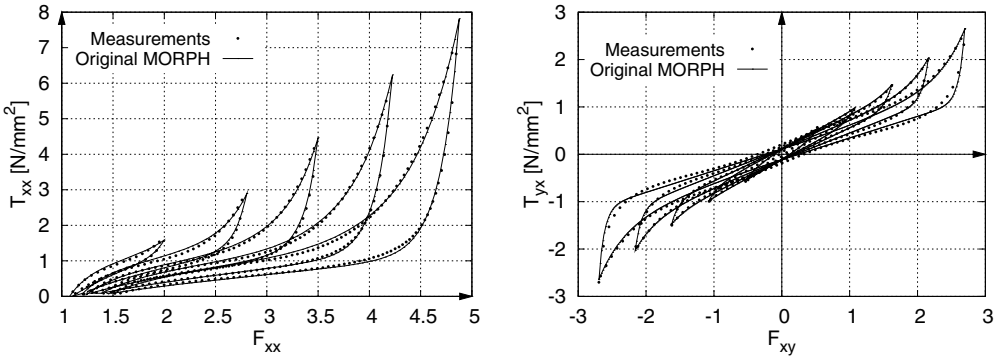

Fig. 3.3 Simultaneous adaptation of the MORPH constitutive model to uniaxial tension measurements (left) and simple shear measurements (right).

The described parameter identification was also done with the new concept using the one-dimensional stress-strain behavior of the original MORPH model within the representative directions. As shown in Fig. 3.4 the resulting generalized constitutive model can also be adapted very well to the experiments while still exhibiting all the inelastic material characteristics of the input model. Even in the case of the simple shear deformation none of the typical characteristics have been getting lost or falsified. In fact this is quite remarkable because the one-dimensional stress-strain relation does not include any information about the material behavior concerning shear deformations. Thus, the material behaviour of the original model concerning complex loads can be well estimated by using the computation with representative directions only.

Besides the inelastic MORPH constitutive model the concept of representative directions has also been applied to rheological material models. In this paper the task is restricted to a Maxwell model as illustrated in Fig. 3.5. In the following the hyperelastic material behavior of the Neo-Hooke model is used for both springs while the dashpot is assumed to react proportional to the strain rate.

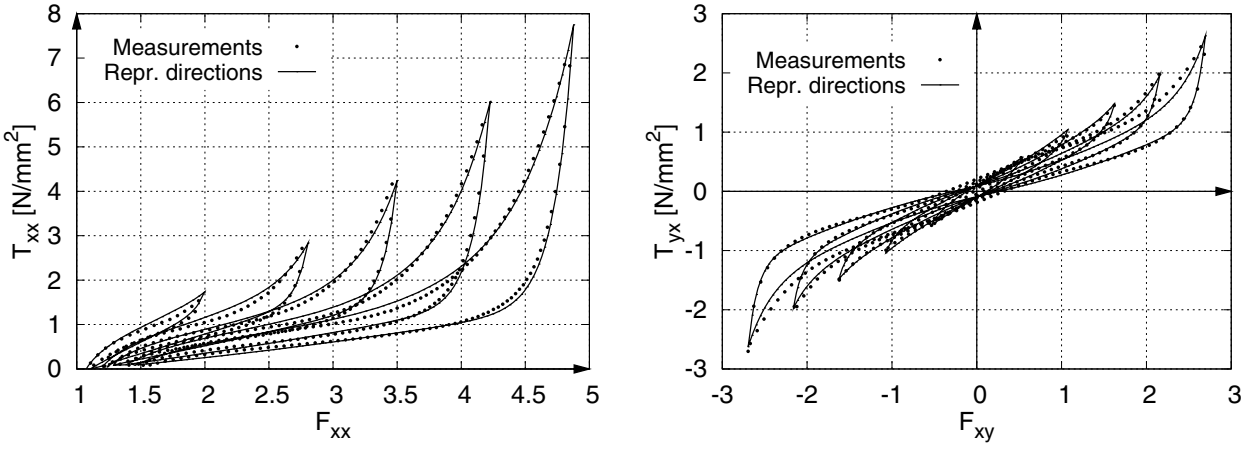

Fig. 3.4 Simultaneous adaptation of the MORPH model within representative directions to uniaxial tension measurements (left) and simple shear measurements (right).

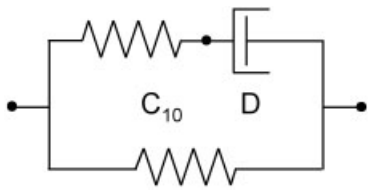

Fig. 3.5 Maxwell model for uniaxial tension with two hyperelastic springs and a linear dashpot.

Provided, that the virtual cross sections of the elements are all set to be equal, the total first Piola-Kirchhoff stresses of this one-dimensional system result as the sum of the single stress contributions of the Maxwell element and the parallel spring. The stress response of the viscoelastic Maxwell element has to be calculated numerically by solving a differential equation for the elongation $\overset{\alpha}{\lambda}_{\text{Sp}}$ of the spring which represents an internal variable of this rheological material model:

$$\overset{\alpha}{T} = \overset{\alpha}{T}_{\text{Maxwell}} + 2\,C_{10}\left(\overset{\alpha}{\lambda} - \frac{1}{\overset{\alpha}{\lambda^2}}\right) \quad \text{with} \quad \overset{\alpha}{T}_{\text{Maxwell}} = 2\,C_{10}\left(\overset{\alpha}{\lambda}_{\text{Sp}} - \frac{1}{\overset{\alpha^2}{\lambda}_{\text{Sp}}}\right) \quad . \tag{3.10}$$

The transmission of the viscoelastic characteristics of this one-dimensional material description to the constitutive model resulting from the concept of representative directions can be verified by simulating a stress relaxation and a creep test demonstrating the time dependency of the material model (see Fig. 3.6). To verify some aspects of plausibility the simulations were accomplished by varying the proportionality constant D between the reaction force and the velocity of the dashpot while the parameter C_{10} is set to be equal for both springs. The stress relaxation test begins with an instantaneous deformation which remains constant over the whole loading process. Due to the viscous behavior of the dashpot the elongation of the spring within the Maxwell element decreases, so that the total stresses converge to a constant value determined by the parameter C_{10} of the parallel spring. Furthermore the constant D shows an effect on the initial stress value for $t = 0$ s as well as the curvature of the relaxation curve. In contrast to this the creep test is characterized by an instantly applied stress value which results in an increasing deformation of the system until the Maxwell element is completely released and the external load is exclusively carried by the parallel spring.

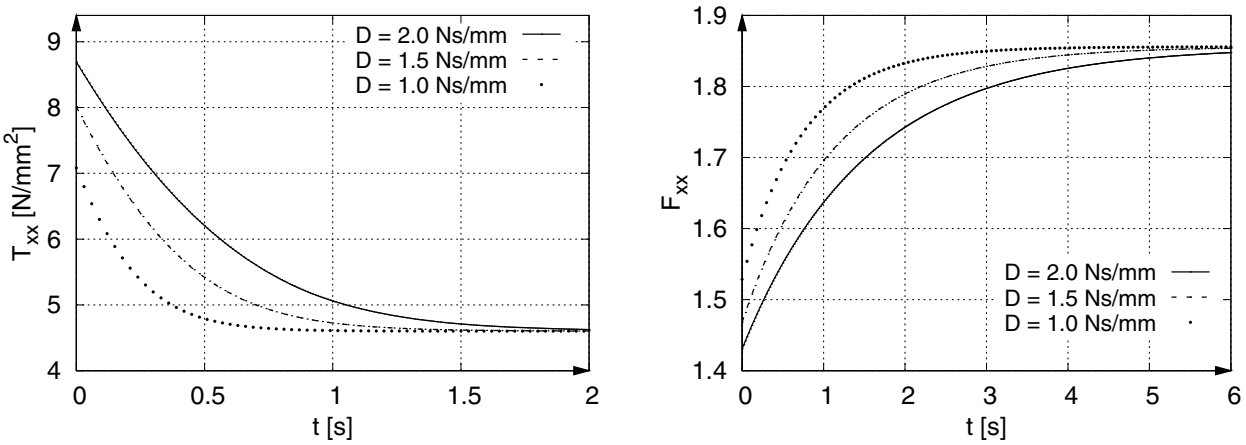

Fig. 3.6 Simulation of a stress relaxation test (left) and a creep test (right) using a Maxwell model in representative directions.

Another loading process, that exhibits the viscoelastic behavior of the constitutive model, is a simple shear deformation with rotating axes as depicted in Fig. 3.7. At the beginning of the process the element is charged with a shear deformation F_{xy} which results in a certain stress response σ_{xy} depending on the constant D of the dashpot. Then the shear direction is rotated in a circle while keeping the shear amplitude always constant, so that the stress components σ_{xy} and σ_{yz} are alternating periodically. Due to the influence of the viscous part of the material model the rotation process starts with a transitional phase characterized by a decreasing stiffness, whereas the duration of that period depends on the parameter D again. After having reached a steady state all invariants of the strain tensor and the stress tensor remain constantly. Nevertheless, the inelastic material behavior effects a dissipation of energy all the time which results in a difference between the shear direction and the direction of the corresponding shear stress.

The mechanical behavior of the Maxwell model within representative directions was also compared with a standard Maxwell model provided by the finite element program ABAQUS. In fact, this original constitutive model is restricted to a linear spring within the Maxwell element. Thus, the input model for the concept of representative directions has been modified in this respect. In addition to the simulations illustrated above, uniaxial tension tests and simple shear tests were carried out. For all of these deformation processes both material models exhibit a qualitatively similar material behavior considering all of the visco-elastic characteristics. Thus, the concept of representative directions appears to be well suitable also for this special kind of material class.

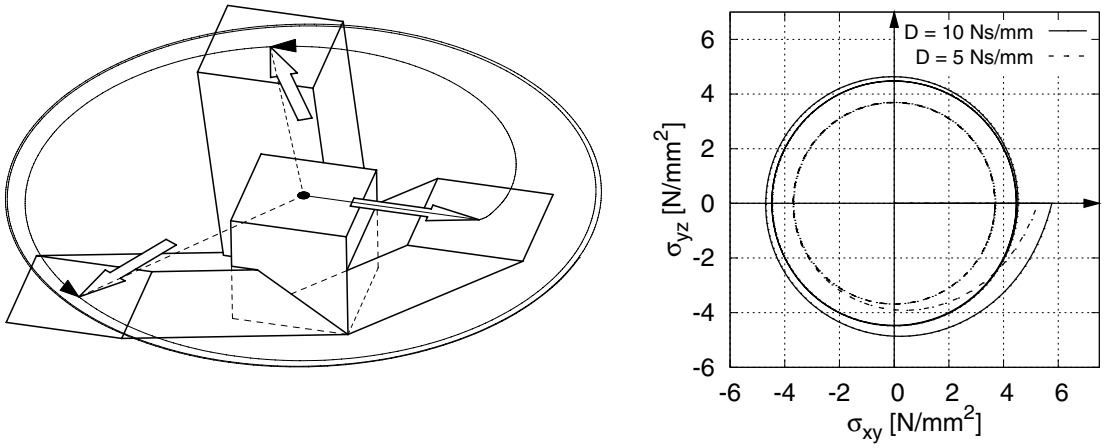

Fig. 3.7 Simulation of a simple shear process with rotating axes using a Maxwell model in representative directions.

4 Methods for increasing the numerical efficiency

4.1 Uniform distribution of the representative directions

The numerical computation of the stress tensor $\underline{\underline{\widetilde{T}}}$ according to Eq. (2.14) causes a dependence of the resulting material behavior on the current orientation of the unit vectors $\overset{\alpha}{\underline{e}}$ as a result of the deviation from the integral over continuously distributed directions in space. The highest possible approximation error for a given number of directions as a measure of the induced anisotropy can be minimized by distributing the representative directions as uniformly as possible in combination with the use of appropriate weighting factors. An analytical solution for this problem is only given by the five Platonic solids, whereas the icosahedron with its 20 congruent triangles provides the largest number ($n = 10$) of evenly distributed directions in space (see Fig. 4.1). As a consequence of this uniform distribution the ten directions are all scaled with the same weighting factor $\overset{\alpha}{w} = 1/10$.

Fig. 4.1 Ten evenly distributed directions in space given by the normals of the surface areas of an icosahedron, respectively by the vertices of a dodecahedron.

Even though the normals of the icosahedron are perfectly distributed in space the number of $n = 10$ might not be high enough to minimize the undesirable anisotropy in order to perform an accurate finite element simulation (see Sect. 4.2). But concerning larger numbers there only exist numerical solutions for this problem, so that the directions cannot be distributed perfectly uniform any more and the associated weighting factors have to be specified individually for each single direction in space. A common approach, which is suggested by Pawelski [15] and also applied by Diani et al. [4], is to divide the surface areas of the icosahedron in N^2 further triangles (with $N = 2, 3, 4, ...$) in order to use the normals as representative directions and the surface areas of the triangles as corresponding weighting factors. In contrast to this Lulei [12] and Miehe et al. [13] use a set of 21 directions that was proposed by Bazant and Oh [1] using a numerical optimization algorithm.

Both of these approaches have the disadvantage that the application is exclusively limited to certain numbers of directions. Furthermore the method proposed by Pawelski [15] is characterized by a decreasing efficiency for large numbers of subdivisions because the difference between the surface areas of the generated triangles is increasing rapidly. The idea of creating new polyhedrons by subdividing Platonic solids is just one example of the numerous approaches for an efficient

numerical integration over the surface of the sphere. In this context the main problem is the lack of an exact measure for a uniform distribution, so that many different criteria for this quality have been developed (e.g. Conway and Sloane [3], Saff and Kuijlaars [16]). Thus, each numerical algorithm for distributing points and calculating the corresponding weighting factors is based on the minimization of such a criterion which is often of a rather mathematical meaning (Sloan and Womersley [19], Fliege and Maier [5]).

In this paper we suggest an algorithm related to the so-called Thomson problem (Thomson [20]). The idea is to place any given number of points on the surface of a unit sphere which are modeled as electric charges repelling each other according to Coulomb's law while permanently bonded to the surface of the sphere. The initial distribution is created by applying a random generator to the spherical coordinates ϑ and φ of the associated unit vectors $\overset{\alpha}{\underline{e}}$. During the process of iteration the minimization of the total force of the whole system finally leads to an equilibrium where the unit vectors are considered to be distributed in space as uniformly as possible. For the use within the concept of representative directions the described algorithm has to be modified in such a way that two opposite electric charges are permanently coupled during the optimization process, so that a symmetric distribution relative to the center of the sphere is secured. This is necessary because the uniaxial stresses along the representative directions $\overset{\alpha}{\underline{e}}$ always relate to the opposite directions $-\overset{\alpha}{\underline{e}}$ too. As an example Fig. 4.2 shows the distribution of 2×50 points concerning their starting position (left) and their optimized position (right).

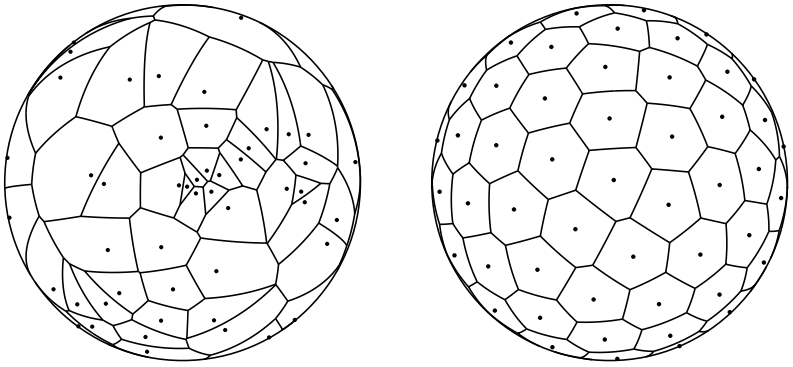

Fig. 4.2 Distribution of 2×50 points on the surface of the unit sphere to use as representative directions with Voronoi cells as corresponding weighting factors.

Fig. 4.2 also depicts a so-called Voronoi diagram consisting of single polygons (Voronoi cells) which are constructed around the points on the surface of the sphere by using a numerical algorithm of Sugihara [18]. The special characteristic of a Voronoi diagram is that any point within a single cell is closer to the associated central point than to the central point of any other polygon, so that a characteristic region is assigned to each position on the sphere. Thus, it seems to be appropriate to use the surface areas of these Voronoi cells as weighting factors for the representative directions (see Eq. (2.14)). The calculation of these surface areas is achieved by dividing each polygon into spherical triangles which are defined by the vertices of the polygon and the associated central point. Finally, the surface area of the Voronoi cell is obtained by adding the surface areas of these triangles which are determined by the angles between the three position vectors of their vertices. To check the correctness of this computation the numerical algorithm should verify whether the sum of all Voronoi cells is equal to the surface area of the unit sphere.

4.2 Computation of the stress tensor by using averaged elongations

Another possibility to reduce the anisotropy caused by the error of the numerical integration for a specific number of representative directions might be the computation of the uniaxial stresses $\overset{\alpha}{\widetilde{T}}$ by means of those elongations

$$\overset{\alpha}{\lambda}_m = \sum_{\beta=1}^{i} \overset{\alpha\beta}{w}\,\overset{\alpha\beta}{\lambda} \quad \text{with} \quad \overset{\alpha\beta}{\lambda} = \sqrt{\overset{\alpha\beta}{\underline{e}} \cdot \overset{G}{\underline{\underline{C}}} \cdot \overset{\alpha\beta}{\underline{e}}} \tag{4.1}$$

that are averaged over several elongations $\overset{\alpha\beta}{\lambda}$ within a Voronoi cell. For this purpose each Voronoi cell α is divided into a certain number i of subcells β, whereas the surface areas of these spherical subcells are used as weighting factors for the individually chosen directions of the additional elongations. In the following the method will be tested by using the subdivided triangles of the icosahedron (see Fig. 4.3). The chosen positions of these four integration points within the

triangle might not be optimal concerning an efficient numerical integration, but for the first step it seems to be the easiest way to determine the associated weighting factors.

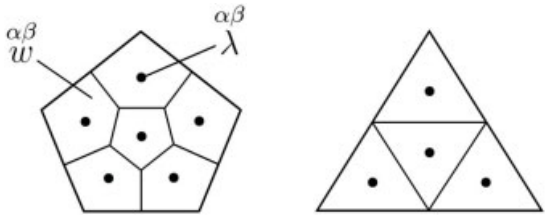

Fig. 4.3 Subdivision of Voronoi cells for calculating averaged elongations.

The resulting second Piola-Kirchhoff stress tensor $\widetilde{\underline{\underline{T}}}$ is finally obtained by postulating the equivalence of stress power as already described in Sect. 2.1 which leads to a modified version of Eq. (2.14):

$$\widetilde{\underline{\underline{T}}} = \sum_{\alpha=1}^{n} \left[\overset{\alpha}{w}\, \overset{\alpha}{\widetilde{T}}\, \overset{\alpha}{\lambda}_m \sum_{\beta=1}^{i} \begin{pmatrix} \overset{\alpha\beta}{w} \\ \overset{\alpha\beta}{\lambda} \end{pmatrix} \underline{\overset{\alpha\beta}{e}} \circ \underline{\overset{\alpha\beta}{e}} \right] \quad \Rightarrow \quad \widetilde{T}_{ab} = \sum_{\alpha=1}^{n} \left[\overset{\alpha}{w}\, \overset{\alpha}{\widetilde{T}}\, \overset{\alpha}{\lambda}_m \sum_{\beta=1}^{i} \begin{pmatrix} \overset{\alpha\beta}{w} \\ \overset{\alpha\beta}{\lambda} \end{pmatrix} \overset{\alpha\beta}{e}_a \overset{\alpha\beta}{e}_b \right] \quad . \tag{4.2}$$

The effect of using averaged elongations is quite similar to the increase of the number of representative directions, but the amount of computational cost is much less because it is comparatively easier to compute additional elongations than to solve the whole one-dimensional material model in those directions. The advantage of this method can be demonstrated by simulating uniaxial tension tests while rotating the tensile axis relatively to the fixed representative directions. Due to the approximation error of the numerical integration the tensile stress depends on the current orientation of the tensile axis, so that the amount of the total discrepancy can be interpreted as a measure for the anisotropy given by the respective set of representative directions. Fig. 4.4 shows the difference between the minimum and the maximum stress value in relation to the isotropic stress value (exact solution of the integral in Eq. (2.13)) using the Neo-Hooke model within the ten representative directions of the icosahedron.

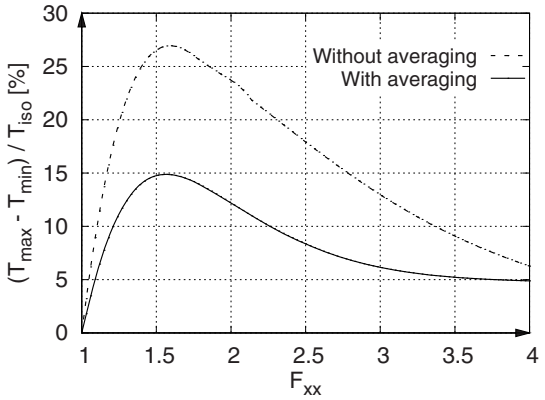

Fig. 4.4 Reduction of the discrepancy of the tensile stress with respect to the rotation of the tensile axis by using averaged elongations.

Obviously the approximation error of the numerical integration can already be reduced significantly by using only four elongations within each triangle of the icosahedron. Besides the discrepancy of the tensile stress the anisotropy has a second effect. For some orientations of the tensile axis the deformation gradient exhibits shear components as displayed by the cross sectional area of the finite element for an external deformation of $F_{xx} = 3$ (see Fig. 4.5a).

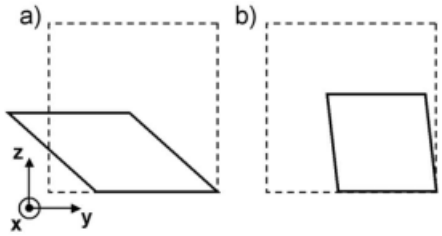

Fig. 4.5 Shear deformation of a finite element for a uniaxial tension test simulated with the original algorithm (a) and with the usage of averaged elongations (b).

As shown in Fig. 4.5b the usage of averaged elongations reduces this immense shear deformation of the element since the cross-sectional area is nearly quadratic like in the case of isotropic material behavior. Nevertheless the discrepancy of the tensile stress makes clear that even with averaged elongations the ten representative directions of the icosahedron are still insufficient to provide for an accurate numerical integration. Thus, concerning the application within the finite element

method the averaged elongations must be necessarily calculated by subdividing the irregular Voronoi cells, even though the determination of the integration points for an efficient integration over these spherical polygons might not be that simple. Furthermore it has to be mentioned that the method of averaged elongations itself is still in a development phase, but at least these first results indicates a worthwhile modification of the original algorithm.

4.3 Efficient computation of the material tangent

The concept of representative directions is already implemented into the finite element programs ABAQUS and MSC. MARC. First the implementation has been accomplished by using the subroutine *HYPELA2* of MSC.MARC which relates to the Lagrangean formulation. To limit the amount of work the implementation into ABAQUS via the user subroutine *UMAT* has been done by using a special algorithm of Ihlemann [11] to convert the Lagrangean material tangent into its Eulerian equivalent. Considering Eq. (2.38) in combination with Eq. (2.8) the material tangent of the complete constitutive model according to the Lagrangean formulation is defined as follows:

$$\underset{\equiv\equiv\equiv\equiv}{K} = \underset{\equiv\equiv\equiv\equiv}{\overset{1}{K}} + \underset{\equiv\equiv\equiv\equiv}{\overset{2}{K}} = 2\,\frac{\partial\left[\left(\underset{\equiv\equiv}{\widetilde{T}}^{*}\cdot\underset{\equiv\equiv}{\overset{G}{C}}\right)'\cdot\underset{\equiv\equiv}{C}^{-1}\right]}{\partial\underset{\equiv\equiv}{C}} - 2\,\frac{\partial\left[p\,J_3\,\underset{\equiv\equiv}{C}^{-1}\right]}{\partial\underset{\equiv\equiv}{C}} \quad . \tag{4.3}$$

The second part of the stress tensor is a function of the hydrostatic pressure p which depends on the respective finite element program. In case of a linear function

$$p = -K\,(J_3 - 1) \tag{4.4}$$

as used in ABAQUS the differentiation yields

$$\underset{\equiv\equiv\equiv\equiv}{\overset{2}{K}} = \left[2\,K{J_3}^2 - KJ_3\right]\underset{\equiv\equiv}{C}^{-1}\circ\underset{\equiv\equiv}{C}^{-1} + 2\left[K{J_3}^2 - KJ_3\right]\frac{\partial\underset{\equiv\equiv}{C}^{-1}}{\partial\underset{\equiv\equiv}{C}} \quad . \tag{4.5}$$

Within this equation the derivative of the inverse right Cauchy-Green tensor is given by

$$\frac{\partial\underset{\equiv\equiv}{C}^{-1}}{\partial\underset{\equiv\equiv}{C}} = -\frac{1}{2}\left(C^{-1}_{ac}\,C^{-1}_{db} + C^{-1}_{ad}\,C^{-1}_{cb}\right)\ \underline{e}_a\circ\underline{e}_b\circ\underline{e}_c\circ\underline{e}_d \tag{4.6}$$

as stated by Holzapfel [9] or Ihlemann [11]. On the other hand the finite element system MSC.MARC uses a nonlinear function

$$p = -3\,K{J_3}^{-\frac{2}{3}}\left(J_3^{\frac{1}{3}} - 1\right) \tag{4.7}$$

for the hydrostatic pressure which leads to the material tangent

$$\underset{\equiv\equiv\equiv\equiv}{\overset{2}{K}} = \left[2\,K{J_3}^{\frac{2}{3}} - K{J_3}^{\frac{1}{3}}\right]\underset{\equiv\equiv}{C}^{-1}\circ\underset{\equiv\equiv}{C}^{-1} + 6\left[K{J_3}^{\frac{2}{3}} - K{J_3}^{\frac{1}{3}}\right]\frac{\partial\underset{\equiv\equiv}{C}^{-1}}{\partial\underset{\equiv\equiv}{C}} \quad . \tag{4.8}$$

Considering Eq. (4.3) it becomes obvious that the development of a complete tensorial formulation for the derivation of the first part of the stress tensor $\underset{\equiv\equiv}{\widetilde{T}}$ is not that simple. Thus, this task is still in progress, but at least there can be shown the derivation

$$\underset{\equiv\equiv\equiv\equiv}{K}^{*} = 2\,\frac{\partial\underset{\equiv\equiv}{\widetilde{T}}^{*}}{\partial\underset{\equiv\equiv}{C}} = \frac{w}{2\pi}\int_0^{2\pi}\int_0^{\pi}\underset{}{\overset{\alpha}{e}}\circ\underset{}{\overset{\alpha}{e}}\circ\frac{\partial\overset{\alpha}{\widetilde{T}}}{\partial\underset{\equiv\equiv}{C}}\,\sin\vartheta\,\mathrm{d}\vartheta\,\mathrm{d}\varphi = \frac{w}{2\pi}\int_0^{2\pi}\int_0^{\pi}\underset{}{\overset{\alpha}{e}}\circ\underset{}{\overset{\alpha}{e}}\circ\frac{\partial\overset{\alpha}{\widetilde{T}}}{\partial\overset{\alpha}{\lambda}}\frac{\partial\overset{\alpha}{\lambda}}{\partial\underset{\equiv\equiv}{C}}\,\sin\vartheta\,\mathrm{d}\vartheta\,\mathrm{d}\varphi \tag{4.9}$$

of the intermediate stress tensor $\underset{\equiv\equiv}{\widetilde{T}}^{*}$ as a part of it (see Eq. (2.16)) while the outer derivation is still solved separately for each coefficient. Unlike Eq. (2.17) the elongations $\overset{\alpha}{\lambda}$ referring to the extended version of the algorithm are merely calculated with the isochoric right Cauchy-Green tensor $\underset{\equiv\equiv}{\overset{G}{C}}$:

$$\underset{\equiv\equiv\equiv\equiv}{K}^{*} = \frac{w}{2\pi}\int_0^{2\pi}\int_0^{\pi}\underset{}{\overset{\alpha}{e}}\circ\underset{}{\overset{\alpha}{e}}\circ\frac{\partial\overset{\alpha}{\widetilde{T}}}{\partial\overset{\alpha}{\lambda}}\frac{1}{2\overset{\alpha}{\lambda}}\frac{\partial\left(\underset{}{\overset{\alpha}{e}}\cdot\underset{\equiv\equiv}{\overset{G}{C}}\cdot\underset{}{\overset{\alpha}{e}}\right)}{\partial\underset{\equiv\equiv}{C}}\,\sin\vartheta\,\mathrm{d}\vartheta\,\mathrm{d}\varphi \tag{4.10}$$

$$= \frac{w}{2\pi} \int_0^{2\pi} \int_0^{\pi} \overset{\alpha}{\underline{e}} \circ \overset{\alpha}{\underline{e}} \circ \frac{\partial \overset{\alpha}{\widetilde{T}}}{\partial \overset{\alpha}{\lambda}} \frac{1}{2\overset{\alpha}{\lambda}} \frac{\partial \left(\overset{\alpha}{\underline{e}} \circ \overset{\alpha}{\underline{e}} \cdot\cdot \overset{G}{\underline{\underline{C}}} \right)}{\partial \underline{\underline{C}}} \sin\vartheta \, \mathrm{d}\vartheta \, \mathrm{d}\varphi \quad .$$

Consequently the derivation

$$\begin{aligned} \frac{\partial \left(\overset{\alpha}{\underline{e}} \circ \overset{\alpha}{\underline{e}} \cdot\cdot \overset{G}{\underline{\underline{C}}} \right)}{\partial \underline{\underline{C}}} &= \overset{\alpha}{\underline{e}} \circ \overset{\alpha}{\underline{e}} \cdot\cdot \frac{\partial \overset{G}{\underline{\underline{C}}}}{\partial \underline{\underline{C}}} \\ &= \overset{\alpha}{\underline{e}} \circ \overset{\alpha}{\underline{e}} \cdot\cdot J_3^{-\frac{2}{3}} \left(\frac{1}{2} \left(\underline{e}_a \circ \underline{e}_b \circ \underline{e}_a \circ \underline{e}_b + \underline{e}_a \circ \underline{e}_b \circ \underline{e}_b \circ \underline{e}_a \right) - \frac{1}{3} \underline{\underline{C}} \circ \underline{\underline{C}}^{-1} \right) \\ &= J_3^{-\frac{2}{3}} \overset{\alpha}{\underline{e}} \circ \overset{\alpha}{\underline{e}} - \frac{1}{3} \overset{\alpha}{\underline{e}} \circ \overset{\alpha}{\underline{e}} \cdot\cdot \overset{G}{\underline{\underline{C}}} \circ \underline{\underline{C}}^{-1} \end{aligned} \tag{4.11}$$

differs from the corresponding expression in Eq. (2.18). Now the expression $\overset{\alpha}{\underline{e}} \circ \overset{\alpha}{\underline{e}} \cdot\cdot \overset{G}{\underline{\underline{C}}}$ can be replaced by the squared elongations $\overset{\alpha}{\lambda}{}^2$:

$$\frac{\partial \left(\overset{\alpha}{\underline{e}} \circ \overset{\alpha}{\underline{e}} \cdot\cdot \overset{G}{\underline{\underline{C}}} \right)}{\partial \underline{\underline{C}}} = J_3^{-\frac{2}{3}} \overset{\alpha}{\underline{e}} \circ \overset{\alpha}{\underline{e}} - \frac{1}{3} \overset{\alpha}{\lambda}{}^2 \underline{\underline{C}}^{-1} \quad . \tag{4.12}$$

Inserting this term into Eq. (4.10) finally yields the demanded tensorial formulation

$$\underline{\underline{\underline{K}}}^* = \frac{w}{4\pi} \int_0^{2\pi} \int_0^{\pi} \frac{\partial \overset{\alpha}{\widetilde{T}}}{\partial \overset{\alpha}{\lambda}} \frac{1}{\overset{\alpha}{\lambda}} \overset{\alpha}{\underline{e}} \circ \overset{\alpha}{\underline{e}} \circ \left(J_3^{-\frac{2}{3}} \overset{\alpha}{\underline{e}} \circ \overset{\alpha}{\underline{e}} - \frac{1}{3} \overset{\alpha}{\lambda}{}^2 \underline{\underline{C}}^{-1} \right) \sin\vartheta \, \mathrm{d}\vartheta \, \mathrm{d}\varphi \tag{4.13}$$

for the derivation of the intermediate stress tensor $\underline{\underline{\widetilde{T}}}^*$. Of course the computation of this tensor with respect to the finite element method requires a numerical approximation for the integral by using a discrete number of directions in space as it was already mentioned concerning the calculation of the stress tensor (see Eq. (2.14)):

$$\underline{\underline{\underline{K}}}^* = \sum_{\alpha=1}^{n} \overset{\alpha}{w} \overset{\alpha}{K} \overset{\alpha}{\underline{e}} \circ \overset{\alpha}{\underline{e}} \circ \left(J_3^{-\frac{2}{3}} \overset{\alpha}{\underline{e}} \circ \overset{\alpha}{\underline{e}} - \frac{1}{3} \overset{\alpha}{\lambda}{}^2 \underline{\underline{C}}^{-1} \right) \quad . \tag{4.14}$$

Furthermore the differentiation of the uniaxial stresses $\overset{\alpha}{\widetilde{T}}$ with respect to the elongations $\overset{\alpha}{\lambda}$ is part of the material tangent

$$\overset{\alpha}{K} = 2 \frac{\partial \overset{\alpha}{\widetilde{T}}}{\partial \overset{\alpha}{C}} = \frac{\partial \overset{\alpha}{\widetilde{T}}}{\partial \overset{\alpha}{\lambda}} \frac{1}{\overset{\alpha}{\lambda}} \tag{4.15}$$

of the one-dimensional input model within each representative direction. In case of simple elastic material models there still might exist an exact solution for this one-dimensional material tangent $\overset{\alpha}{K}$, so that the stress tensor $\underline{\underline{\widetilde{T}}}^*$ can be differentiated completely analytically. But in general the concept is to be applied to inelastic material behavior, so that this quantity has to be calculated numerically by means of a difference quotient. In fact the uniaxial stress-strain relation remains the only part of the constitutive model that is differentiated numerically. This enables an easy extension of the concept with additional one-dimensional material models.

The advantage of this almost analytical differentiation over a complete numerical differentiation of the first part of the stress tensor (see Eq. (4.3)) is a considerable reduction of the simulation runtime and of course a certain gain of numerical stability. The increase of the efficiency concerning computational costs is proportional to the number of representative directions. For example a simulation based on an FE-model with 1000 elements including the hyperelastic Ogden model (Ogden [14]) with six material parameters within 75 representative directions has shown that the simulation runtime with the almost analytical material tangent is nearly 3,5 times less than in case of a complete numerical differentiation.

5 Finite element simulations

The FE-implementation of the algorithm has been tested via numerous simulations using both finite element systems. In the following the illustration is restricted to the results of a simulated rubber wheel which is used by Grosch [6] to measure the friction of elastomers (see Fig. 5.1). In the first loading step a constant force F_y is applied quasi statically to the axis of the wheel to generate a contact with the ground. For this purpose the complete inner area of the wheel is coupled with the axis as a rigid rim. In the next step the axis is moved towards the horizontal direction, so that the wheel starts to rotate due to the Coulomb friction modeled in the contact area. In the following there will be shown the results of the original MORPH constitutive model (compare Hohl [8]) as well as the one-dimensional MORPH model in 50 representative directions using the optimized material parameters resulting from the adaptations of both models to the measurements (see Figs. 3.3 and 3.4).

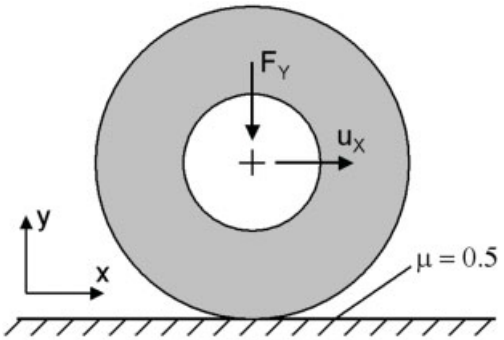

Fig. 5.1 Boundary conditions of the Grosch wheel.

The first results of this ABAQUS simulation are depicted in Fig. 5.2 where the vertical displacement of the axis is plotted against the rotation angle. The similarity between both material models concerning this measurable quantity is quite remarkable, though there remains a certain quantitative difference. Since the applied vertical force leads to comparatively low deformations of the material, this discrepancy might already result from the different material behavior concerning the first loading cycle due to the parameter optimization. The characteristic of the displacement curves shows that during the first revolution the wheel pushes itself back vertically, an effect which probably results from the friction conditions in the contact area in combination with the inelastic material behavior. But at the end of the revolution ($\varphi = 360^{\circ}$) the displacement of the axis increases rapidly because the current material in the contact area has already been softened at the beginning of the loading process. It can be clearly noticed how the stress softening is still continuing after the first revolution until a steady state is reached.

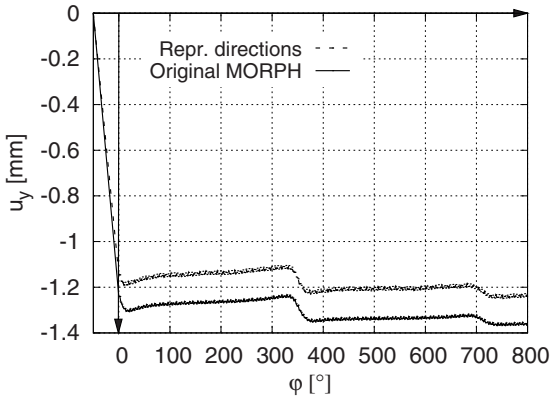

Fig. 5.2 Vertical displacement of the axis of the Grosch wheel during the process of rotation.

In case of the original MORPH constitutive model the effect of stress softening during the loading process can be visualized in form of the quantity C_T^H (see Eq. (3.4)) which is evaluated for each integration point of the finite element mesh (see Fig. 5.3). Within the concept of representative directions the internal variable C_T^H is defined for each single direction $\overset{\alpha}{\underline{e}}$, so that a comparison between both material models concerning the stress softening seems to be difficult. Thus, for a first approach this quantity is averaged over the representative directions, so that one single value

$$C_T^{H^*} = \sum_{\alpha=1}^{n} \overset{\alpha}{w}\, \overset{\alpha}{C_T^H} \tag{5.1}$$

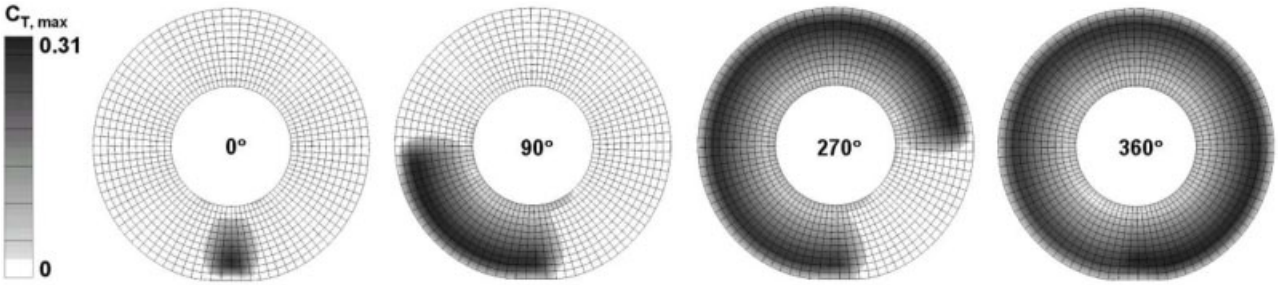

Fig. 5.3 Stress softening within the rotating Grosch wheel simulated with the original MORPH constitutive model.

can be provided for each integration point. Due to the assignment of the stress softening to the representative directions the generalized MORPH material model is characterized by an anisotropic Mullins effect (in contrast to the original MORPH constitutive model) which in fact coincides with the mechanical behavior of real elastomers as shown very clearly by certain experiments (Besdo et al. [2]). This means a great advantage of the concept because this stress-induced anisotropy does not have to be modeled separately but is automatically generated by the use of the inelastic behavior of the MORPH model within different directions in space. If desired, the anisotropic stress softening can also be neutralized to an isotropic Mullins effect by adapting the different values $\overset{\alpha}{C}{}_T^H$ of the representative directions to the maximum value of the most softened material line. Anyway, the averaging of this quantity obviously enables the visualization of the stress softening in a very similar way compared to the original MORPH constitutive model (see Fig. 5.4).

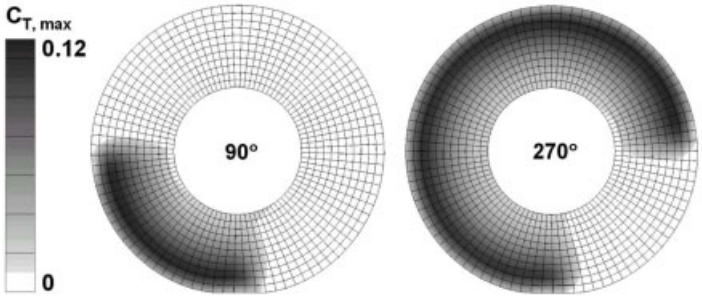

Fig. 5.4 Stress softening within the rotating Grosch wheel simulated with the MORPH model in representative directions.

This ABAQUS simulation is just a first approach to analyze the resulting material behaviour of the new algorithm concerning inhomogeneous stress conditions within a complex finite element model. Especially the use of the inelastic MORPH model within representative directions requires further investigations to understand the effects illustrated above. Nevertheless these first results already indicate that the new algorithm is well suitable for the application within the finite element method.

Finally, it should be mentioned that in case of the generalized MORPH model the usage of 50 representative directions (see Fig. 4.2) already yields a good approximation of the numerical integration. In this case the simulation runtime is about 1.5 times higher than in case of the original MORPH constitutive model. In order to get a similar amount of computational effort the number of representative directions must be reduced to $n = 25$, even though the quality of the numerical integration concerning isotropy decreases accordingly. Thus, the increase of the numerical efficiency of the algorithm is still a remaining task for the future.

6 Conclusions

The development of a constitutive model for a certain material class with respect to the finite element method often leads to an intermediate stage which enables the prediction of the material behavior for uniaxial tension only. The remaining generalization of such a one-dimensional material description to a complete three-dimensional constitutive model, which is able to predict the material behavior for any loading process, might be very difficult and often takes a lot of time. Thus, in such a situation it would be helpful to find a sufficient approximation of the prospective general behavior of a constitutive model by predicting the material behavior for uniaxial tension only. This is the idea of the concept of representative directions which has primarily been developed for industrial applications. The new algorithm is applicable to any model which is able to describe uniaxial loadings, even to those for inelastic material behavior without knowing the free energy. The typical characteristics of the respective material class are generalized in a remarkable similarity to the input model.

The concept is based on the selection of evenly distributed directions in space. Due to the external deformation of each material point the resulting elongations along those representative directions can be used to calculate the corresponding uniaxial stress responses according to the one-dimensional material model. The demand, that all uniaxial stress contributions achieve the same stress power as the overall stress tensor concerning the actual deformation, finally leads to a constitutive model describing the complete tensorial correlation between the stress condition and the associated strain condition. This generalization of one-dimensional material models may be completely automated which is an important requirement for the application within the finite element method.

To increase the numerical efficiency of the concept the representative directions are distributed as uniformly as possible by means of a special algorithm simulating repelling charges on the surface of the sphere while using Voronoi cells as weighting factors for the individual directions in space. Furthermore the anisotropy caused by the approximation error of the numerical integration can be reduced significantly by calculating the uniaxial stresses with those elongations that are averaged over several elongations within each Voronoi cell. Concerning the implementation into the finite element method the computation of the material tangent is based on an almost analytical differentiation of the stress tensor which results in a remarkable reduction of the simulation runtime compared to a full numerical differentiation. The new algorithm has been implemented into the finite element systems ABAQUS and MSC.MARC via the corresponding user interfaces *UMAT* and *HYPELA2*. This enables simulations of inhomogeneous stress conditions within technical components, though the input model predicts uniaxial material behavior only.

References

[1] Z. P. Bazant and B. H. Oh, Efficient numerical integration on the surface of a sphere, Z. Angew. Math. Mech. **66**(1), 37–49 (1986).
[2] D. Besdo, J. Ihlemann, J. G. R. Kingston, and A. H. Muhr, Modelling Inelastic Stress-strain Phenomena and a Scheme for Efficient Experimental Characterization, in: Constitutive Models for Rubber III, edited by J. Busfield and A. Muhr (Balkema, Lisse, 2003) pp. 309–317.
[3] J. H. Conway and N. J. Sloane, Sphere Packings, in: Lattices and Groups (Springer-Verlag, Berlin, Heidelberg, New York, 1998).
[4] J. Diani, M. Brieu, and P. Gilormini, Observation and modeling of the anisotropic visco-hyperelastic behavior of a rubberlike material, Int. J. Solids Struct. **43**, 3044–3056 (2005).
[5] J. Fliege and U. Maier, The distribution of points on the sphere and corresponding cubature formulae, IMA J. Numer. Anal. **19**, 317–334 (1999).
[6] K. A. Grosch, Laborbestimmung der Abrieb- und Rutschfestigkeit von Laufflächenmischungen – Teil I: Rutschfestigkeit, Kautschuk und Gummi, Kunststoffe **49**, 432–441 (1996).
[7] G. Heinrich, M. Klüppel, and T. Vilgis, Reinforcement Theories, in: Physical Properties of Polymers Handbook, edited by J. E. Mark (Springer-Verlag, Berlin, Heidelberg, New York, 2007).
[8] C. Hohl, Anwendung der Finite-Elemente-Methode zur Parameteridentifikation und Bauteilsimulation bei Elastomeren mit Mullins-Effekt (VDI-Verlag, Düsseldorf, 2007).
[9] G. A. Holzapfel, Nonlinear Solid Mechanics – A Continuum Approach for Engineering (Wiley, Chichester, 2000).
[10] J. Ihlemann, Kontinuumsmechanische Nachbildung hochbelasteter technischer Gummiwerkstoffe (VDI-Verlag, Düsseldorf, 2003).
[11] J. Ihlemann, Beobachterkonzepte und Darstellungsformen der nichtlinearen Kontinuumsmechanik. Habilitationsschrift (Leibniz Universität, Hannover, 2007).
[12] F. Lulei, Mikromechanisch motivierte Modelle zur Beschreibung finiter Deformationen gummiartiger Polymere: Physikalische Modellbildung und numerische Simulation, Dissertation (Universität Stuttgart, 2002).
[13] C. Miehe, S. Göktepe, and F. Lulei, A micro-macro approach to rubber-like materials – Part I: the non-affine micro-sphere model of rubber elasticity, J. Mech. Phys. Solids **52**, 2617–2660 (2004).
[14] R. W. Ogden, Large deformation isotropic elasticity – on the correlation of theory and experiment for incompressible rubberlike solids, Proc. R. Soc. Lond. A **326**, 565–584 (1972).
[15] H. Pawelski, Eigenschaften von Elastomerwerkstoffen mit Methoden der statistischen Physik (Shaker-Verlag, Aachen, 1998).
[16] E. B. Saff and A. B. Kuijlaars, Distributing many points on the sphere, Mathematical Intelligencer **6**, 237–265 (1997).
[17] S. Seelecke, Equilibrium thermodynamics of pseudoelasticity and quasiplasticity, Contin. Mech. Thermodyn. **8**, 309–322 (1996).
[18] K. Sugihara, Laguerre Voronoi diagram on the sphere, J. Geom. Graph. **6**, 69–81 (2002).
[19] I. H. Sloan and R. S. Womersley, Extremal Systems of Points and Numerical Integration on the Sphere, Adv. Comput. Math. **21**, 102–125 (2004).
[20] J. J. Thomson, On the structure of the atom: An investigation of the stability and periods of oscillation of a number of corpuscles arranged at equal intervals around the circumference of a circle, Philos. Mag. **6**, 237–265 (1904).